Bay Annulated Indigo as a New Chromophore for p-type Dye-Sensitized Solar Cells

Dr Gareth H. Summers and Dr Elizabeth A. Gibson*

Chemistry: School of Natural and Environmental Science, Newcastle University,

Newcastle upon Tyne, NE1 7RU, UK

Elizabeth.gibson@ncl.ac.uk

Abstract

A prototype bay-annulated indigo dye has been synthesised and applied in p-type dye-sensitized solar cells. The dye produced a broad spectral response up to 700 nm and an encouraging photocurrent (Jsc = 1.13 mA cm^{-2}, IPCE of 6.8%) was recorded. These results have highlighted several challenges for integrating BAI dyes into pDSCs, including, low dye loading, a tendency to aggregate and lack of built-in charge transfer character, which can be overcome by simple modifications to the dye structure.

Introduction

Since O'Regan and Grätzel's seminal paper on dye-sensitized photoelectrochemical cells,[1] an enormous research effort has focused on improving their performance in order to provide a low-cost alternative to conventional photovoltaic devices. Despite this, the maximum reported efficiency for solar cells based on a sensitized TiO_2 photoanode (n-type) has only reached 13-14%.[2–4] Tandem dye-sensitized solar cells, in which the dark counter electrode is replaced with a dye-sensitized photocathode, offer a potential solution to increasing the efficiency.[5] However, the performance of p-type dye-sensitized solar cells (pDSCs), first described by Lindquist and co-workers,[6] lags behind that of the conventional n-type devices.[7] These cells operate along similar principles to nDSCs, but the TiO_2 is replaced with a p-type semiconductor, typically NiO, so the majority charge carriers are positive holes (h+), the electron flow occurs in the reverse (cathodic) direction.[8,9] A schematic representation of a NiO-based pDSC is given in Figure 1. Light absorption by the dye stimulates electron transfer from the valence band of the NiO to the excited dye. A redox mediator (e.g. I_3^-) in solution accepts the electron from the reduced dye and the product (I^-) diffuses to the counter electrode where it is re-oxidised. Recombination reactions typically occur much faster when NiO is used, compared to TiO_2, which is thought to be a cause of the lower efficiency.[10,11]

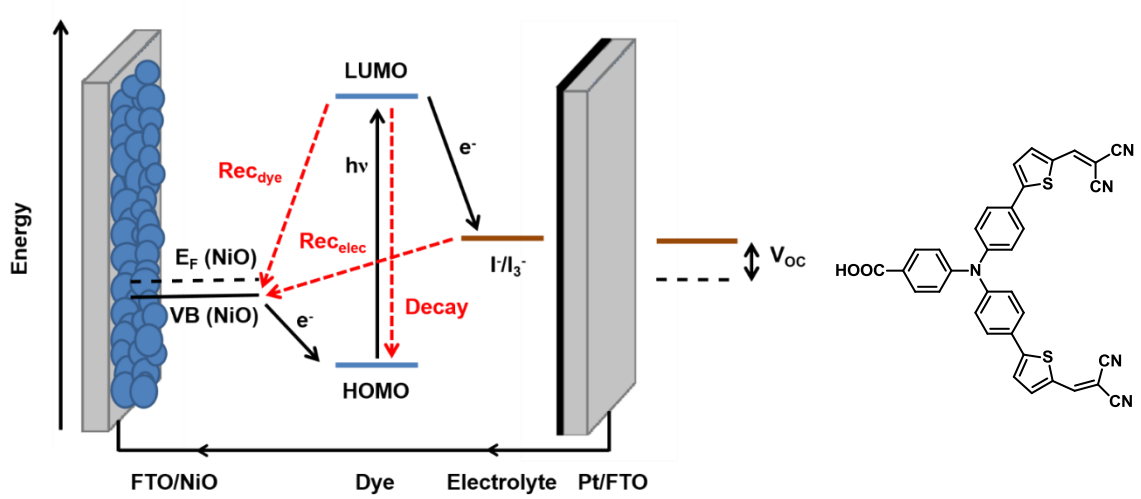

Figure 1. Schematic representation of the charge transfer processes occurring within a NiO-based pDSC and structure of a benchmark dye, **P1**.[12]

As the dye is the part of a DSC that absorbs light and drives the production of a photocurrent, the development of new sensitizers is crucial to improve device efficiencies. There are a number of criteria that need to be considered when designing new dyes. (1) The dye must be capable of absorbing photons in the visible-NIR region, ideally with a broad absorption profile. Due to the typically low NiO film thicknesses used (ca. 1.5 µm), high extinction coefficients are needed to maximise light harvesting. (2) As nDSCs have been optimised to harvest higher energy photons, we require dyes that can absorb across the longer-wavelength visible and near-IR regions for NiO (to construct tandem devices). (3) An anchoring unit, typically a group containing an acidic proton, is also essential for the dye to adsorb onto the semiconductor surface and to facilitate efficient charge injection from NiO to the dye. The most commonly used anchoring units are carboxylic acids,[5,12,13] but phosphonates[14,15] and pyridine[16–18] groups have also been used. (4) The HOMO and LUMO levels of the dye need to be suitably positioned to promote efficient charge injection and dye regeneration. The HOMO needs to be more positive than the valence band edge of NiO and the LUMO needs to be more negative than the redox potential of the electrolyte. (5) As recombination between the excited dye and holes in NiO is so prevalent for pDSCs,[19,20] the dye structure should promote a long-lived charge-separated state. This is usually attempted by following a donor-acceptor 'push-pull' design, where electron density will be shuttled to the periphery of the dye following charge injection from NiO, to increase the spatial electron/hole separation.[5,13,21–23]

One of the oldest known blue dyes is indigo, which is naturally occurring but is now produced synthetically on a large scale for use in the textile industry. The direct use of indigo as a starting material is hindered due to limited solubility, although a structurally similar chromophore, isoindigo, has been applied in pDSCs.[24] The isoindigo core is not readily available and needs to be synthesised in several

steps. Liu *et al.* functionalised indigo by reaction with 2-thienylacetyl chloride to produce bay-annulated indigo (BAI, Figure 2).[25] This unit was incorporated into fluorene and benzodithiophene containing polymers which were used as organic semiconductors. In this derivative, the two pyrrole groups were incorporated into a conjugated, planar structure with two flanking thiophenes. These thiophene units can be easily functionalised through aromatic substitution reactions and the solubility is improved compared to indigo due to the suppression of hydrogen-bonding interactions. Due to increased conjugation, BAI has an extinction coefficient that is higher than indigo (ε = 26 800 M^{-1} cm^{-1} for BAI vs. 22 140 M^{-1} cm^{-1} for indigo).[26] Despite the favourable properties (large extinction coefficient, high solubility and apparent ease of functionalisation), BAI-based dyes have not, until now, been used for either n-type or p-type DSCs. This paper explores the feasibility of applying BAI-based dyes in pDSCs and describes the performance of a prototype dye.

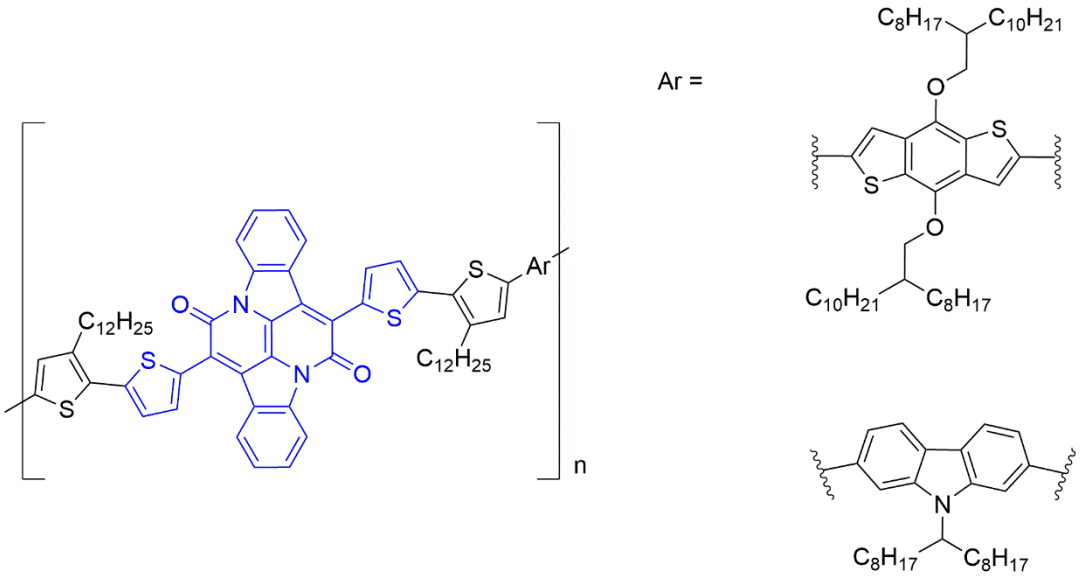

Figure 2. Conjugated polymers based on BAI used as organic semiconductors, synthesised by Liu *et al*. The BAI core is highlighted in blue.

Experimental

General Methods

Products were characterised by ^{1}H NMR and ^{13}C NMR using a Bruker 400, 500 or 700 MHz spectrometer at 25°C; chemical shifts (δ) are reported in parts per million (ppm) from low to high field and referenced to residual non-deuterated solvent. Standard abbreviations indicating multiplicity are used as follows: s = singlet; d = doublet; t = triplet; m = multiplet. Infrared spectroscopy was performed using a Varian 800 FT-IR spectrometer. UV-visible absorption spectroscopy measurements in solution were recorded on either an Ocean Optics USB2000+ VIS-NIR fibre optic spectrometer or a Shimadzu

UV-1800 UV spectrophotometer. All measurements were performed using a quartz cuvette with a path length of 1 cm. Photoluminescence spectroscopy measurements in solution were recorded using a Shimadzu RF-6000 spectro fluorophotometer. All measurements were performed using a quartz cuvette with a path length of 1 cm. Electrochemical studies were carried out using an IviumStat potentiostat controlled using IviumSoft. Redox potentials were determined using differential pulse voltammetry. All electrochemistry was performed under a nitrogen atmosphere using a three-electrode setup in a single compartment cell. A glassy carbon working electrode (modified with BAI-COOH, deposited from $CHCl_3$/TFA (99:1, v:v)), a Pt wire secondary electrode and a saturated calomel reference electrode were used. Measurements were carried out in anhydrous $CHCl_3$ that had been purged with nitrogen. 0.5 M TBA PF_6 supporting electrolyte was used. All redox potentials are quoted against the ferrocenium/ferrocene couple used as an internal standard.

Computational Studies

DFT calculations were performed using Gaussian G09 on the Pople Cluster at Newcastle University. Optimised geometries were first calculated in vacuum, then in solvent (using the PCM). Frequency calculations were used to check that the optimised geometries were true energy minima. Time-dependent DFT (TDDFT) calculations were then performed to calculate the electronic transitions. A B3LYP/6-31G(d,p) exchange functional and basis set combination was used.

Solar Cell Measurements

Conductive glass substrates were cleaned using an ultrasonic bath for 15 minute intervals in various solvents; first in deionised water containing detergents, then in aqueous hydrochloric acid (0.01 M) and finally in ethanol. A NiO precursor solution was prepared by dissolving anhydrous $NiCl_2$ (1 g) and the tri-block co-polymer Pluronic F108 (poly(ethylene glycol)-block-poly(propylene glycol)-block-poly(ethylene glycol)) (1 g) in ethanol (6 g) and Milli-Q water (3 g). Working electrodes were prepared by doctor-blading this precursor solution onto conductive glass substrates (Pilkington TEC15, sheet resistance 15 Ω/square) using Scotch tape as a spacer (0.18 cm^2 active area), followed by sintering in a Nabertherm B150 oven at 450 °C for 30 minutes. NiO films were prepared to a thickness of 1.52 (±0.025) μm, measured using a Bruker DektakXT stylus profilometer and averaged over 3 samples. The NiO electrodes were soaked in a solution of the dye (typically 0.3 mM in acetonitrile) for 16 h at room temperature.

Platinized counter electrodes were prepared by drop-casting (10 μL cm^{-2}) a solution of $H_2PtCl_6 \cdot 6H_2O$ (4.8 mM in ethanol) onto conductive glass (Pilkington TEC8, sheet resistance 8 Ω/square) followed by annealing at 450 °C for 30 minutes. The two electrodes were assembled face-to-face using a 30 μm thick thermoplastic frame (Surlyn 1702, Dyesol). The electrolyte, containing LiI (1.0 M) and I_2 (0.1 M) in anhydrous acetonitrile, was introduced by vacuum back-filling through a pre-drilled hole in the counter electrode, which was sealed afterwards using a glass coverslip.

UV-visible absorption spectra of the dyes adsorbed onto NiO films were recorded using an Ocean Optics USB2000+VIS-NIR fibre-optic spectrophotometer. Current-voltage measurements were performed using an Ivium CompactStat or IviumStat potentiostat under simulated sunlight (AM1.5) from an Oriel VeraSol-2 Class AAA LED Solar Simulator, with an intensity of 100 mW cm^{-2}. Incident photon-to-current conversion efficiencies (IPCE) were recorded using monochromatic light from a 300W Xe lamp (Oriel Newport) fitted with an AM1.5 filter, using a Cornerstone 130 1/8m monochromator and calibrated against a certified reference Si photodiode. Charge lifetimes and densities were recorded at different light intensities upon applying a small square wave modulation to the base light intensity from an LED light source (Ivium ModuLight) and measuring the decay of the voltage or current.

Synthesis.

The synthesis of 1-3 was performed according to the method described by Liu *et al.* with some modifications.[27]

5-((2-ethylhexyl)oxy)-2-nitrobenzaldehyde (1)

5-hydroxy-2-nitrobenzaldehyde (2.5 g, 14.96 mmol, 1 eqv), K_2CO_3 (6.2 g, 44.88 mmol, 3 eqv) and 18-crown-6 (30 mg, 0.11 mmol, 0.75 mol %) were loaded into a 2-neck round bottom flask and purged with 3 vacuum/nitrogen cycles. Anhydrous DMF (30 mL) and 2-ethylhexyl bromide (4.3 g, 22.44 mmol, 1.5 eqv) were added and the mixture was heated at 80 °C for 36 hours. After cooling to room temperature the solution was filtered and evaporated. The product was purified using column chromatography (silica gel, 2:1 petroleum ether/DCM) to give **1** as a light yellow oil (3.97 g, 95 % yield).

^{1}H NMR (400 MHz, $CDCl_3$): δ 10.49 (s, 1H), 8.15 (d, J = 9.1 Hz, 1H), 7.32 (d, J = 2.8 Hz, 1H), 7.14 (dd, J = 9.1, 2.8 Hz, 1H), 3.98 (m, 2H), 1.82-1.72 (m, 1H), 1.52-1.40 (m, 4H), 1.35-1.28 (m, 4H), 0.96-0.89 (m, 6H) ppm.

^{13}C NMR (101 MHz, CDCl3): δ 188.80, 164.00, 142.07, 134.49, 127.36, 118.96, 113.88, 71.92, 39.29, 30.45, 29.10, 23.83, 23.09, 14.16, 11.17 ppm.

IR (neat, ATR): ν = 2959, 2929, 2363, 1699, 1581, 1515, 1462, 1386, 1328, 1285, 1323, 1071, 1016, 848, 748 cm^{-1}.

6,6'-bis((2-ethylhexyl)oxy)-indigo (2)

1 (2.3 g, 8.23 mmol, 1 eqv.) was dissolved in an acetone/water mixture (1/1 v/v, 50 mL) and heated to 60 °C. NaOH (540 mg, 13.5 mmol, 1.6 eqv) dissolved in water (4 mL) was added dropwise over 10 minutes. The solution was heated at 60 °C with vigorous stirring for four hours then cooled to room temperature and poured into 500 mL water. The solution was filtered, washed thoroughly with water then recrystallized from DCM with the addition of petroleum ether to give **2** as a blue solid (570 mg, 13 % yield).

^{1}H NMR (400 MHz, $CDCl_3$): δ 8.71 (s, 2H), 7.19 (d, J = 2.5 Hz, 2H), 7.13 (dd, J = 8.7, 2.6 Hz, 2H), 6.96 (d, J = 8.7 Hz, 2H), 3.84 (d, J = 5.9 Hz, 4H), 1.80-1.67 (m, 2H), 1.53-1.38 (m, 8H), 1.35-1.28 (m, 8H), 0.99-0.87 (m, 12H) ppm.

^{13}C NMR (101 MHz, $CDCl_3$, partial due to low solubility): δ 154.54, 126.02, 113.22, 106.81, 71.58, 39.52, 30.67, 29.22, 24.02, 23.21, 18.59, 14.24, 11.25 ppm.

IR (neat, ATR): ν = 3372, 2958, 2925, 2859, 2339, 1613, 1485, 1467, 1401, 1267, 1223, 1133, 1107, 1063, 816, 778, 694, 525 cm^{-1}.

2,9-Bis((2-ethylhexyl)oxy)-7,14-di(thiophen-2-yl)diindolo-[3,2,1-de:3',2',1'-ij][1,5]naphthyridine-6,13-dione (3)

2 (200 mg, 0.386 mmol) was dissolved in xylene (10 mL) under a nitrogen atmosphere and heated to reflux. 2-Thiopheneacetyl chloride (248 mg, 1.54 mmol, 4 eqv) dissolved in xylene (3 mL) was added dropwise over 30 minutes and then heating was continued for an additional hour. After cooling to room temperature, the solvent was evaporated under reduced pressure and the residue was recrystallized from DCM with the addition of pentane to yield **3** as a purple solid (130 mg, 46 % yield).

^{1}H NMR (400 MHz, $CDCl_3$): δ 8.42 (d, J = 8.9 Hz, 2H), 7.75 (d, J = 3.6 Hz, 2H), 7.70 (dd, J = 5.1, 1.2 Hz, 2H), 7.66 (d, J = 2.5 Hz, 2H), 7.28 (d, J = 3.7 Hz, 2H), 7.10 (dd, J = 9.0, 2.5 Hz, 2H), 3.83 (d, J = 5.8 Hz, 4H), 1.73 (m, 2H), 1.49-1.41 (m, 8H), 1.33 (m, 8H), 0.95-0.90 (m, 12H) ppm.

IR (neat, ATR): ν = 3101, 1958, 1927, 2339, 1623, 1575, 1462, 1445, 1416, 1383, 1352, 1276, 1256, 1223, 1203, 1107, 1077, 1055, 1031, 965, 854, 813, 793, 769, 727, 705, 673, 625 cm^{-1}.

7-(5-bromothiophen-2-yl)-2,9-bis((2-ethylhexyl)oxy)-14-(thiophen-2-yl)diindolo[3,2,1-de:3',2',1'-ij][1,5]naphthyridine-6,13-dione (4)

3 (50 mg, 68.4 µmol, 1 eqv) was dissolved in chloroform (10 mL). NBS (13 mg, 71.8 µmol, 1.1 eqv) was added and the solution was stirred for 2 hours before quenching with the addition of water (50 mL). The organic layer was washed with water then brine, dried using $MgSO_4$ and evaporated. The crude

material was purified using column chromatography (silica gel, DCM) to yield **4** as a purple solid (19 mg, 34 % yield). The bis-brominated product (**5**) was also obtained as a purple solid (20 mg, 33 % yield).

^{1}H NMR (500 MHz, $CDCl_3$): δ 8.30 (d, J = 8.9 Hz, 1H), 8.25 (d, J = 8.9 Hz, 1H), 7.72-7.66 (m, 2H), 7.64 (d, J = 2.5 Hz, 1H), 7.61 (d, J = 2.5 Hz, 1H), 7.50 (d, J = 3.9 Hz, 1H), 7.23 (dd, J = 5.1, 2.6 Hz, 1H), 7.17 (d, J = 3.9 Hz, 1H), 7.04-6.97 (m, 2H), 3.84-3.77 (m, 4H), 1.73 (m, 2H), 1.55-1.39 (m, 8H), 1.34 (m, 8H), 0.98-0.89 (m, 12H) ppm.

^{13}C NMR (101 MHz, $CDCl_3$): δ 158.03, 157.96, 130.51, 130.25, 129.88, 129.73, 129.12, 128.95, 127.01, 126.77, 126.33, 122.29, 118.20, 110.94, 71.54, 39.42, 30.59, 29.23, 23.93, 23.22, 14.28, 11.24 ppm.

IR (KBr, transmittance): ν = 2955, 2926, 2872, 1711, 1624, 1578, 1466, 1447, 1416, 1404, 1383, 1327, 1275, 1246, 1227, 1219, 1202, 1107, 1073, 1030, 978, 854, 822, 795, 768, 733, 698, 673, 571, 503 cm^{-1}.

4-(5-(2,9-bis((2-ethylhexyl)oxy)-6,13-dioxo-14-(thiophen-2-yl)-6,13-dihydrodiindolo[3,2,1-de:3',2',1'-ij][1,5]naphthyridin-7-yl)thiophen-2-yl)benzoic acid (BAI-COOH)

4 (41 mg, 50.6 µmol, 1 eqv), 4-carboxyphenylboronic acid (13 mg, 75.9 µmol, 1.5 eqv), K_2CO_3 (28 mg, 20.24 µmol, 4 eqv) and $Pd(PPh_3)_4$ (3 mg, 2.53 µmol, 5 mol %) were loaded into a Schlenk tube and purged with 3 vacuum/nitrogen cycles. A degassed mixture of dioxane and water (12/3 mL) was added and the solution was heated to 90 °C for 24 hours. After cooling to room temperature, the solvent was evaporated under reduced pressure and the product purified using column chromatography (silica gel, 95:5:1 toluene/methanol/acetic acid) to yield **BAI-COOH** as a blue solid (28 mg, 65 % yield).

^{1}H NMR (700 MHz, $CDCl_3$/TFA): δ 8.38 (d, *J* = 8.8 Hz, 1H), 8.35 (d, *J* = 8.9 Hz, 1H), 8.18 (d, *J* = 8.1 Hz, 2H), 7.84 (d, *J* = 8.2 Hz, 2H), 7.73 (d, *J* = 5.1 Hz, 1H), 7.68 (d, *J* = 3.8 Hz, 1H), 7.65 (d, *J* = 3.7 Hz, 1H), 7.58 (m, 2H), 7.37 (d, *J* = 2.5 Hz, 1H), 7.30 (dd, *J* = 5.2, 3.4 Hz, 1H), 7.16 (m, 2H), 3.86 (d, *J* = 5.9 Hz, 2H), 3.83 (d, *J* = 5.9 Hz, 2H), 1.76 – 1.70 (m, 2H), 1.53 – 1.24 (m, 16H), 0.95 – 0.85 (m, 15H) ppm.

^{13}C NMR (176 MHz, $CDCl_3$): δ 179.63, 158.72, 147.35, 139.57, 137.70, 137.61, 132.96, 132.47, 132.24, 132.08, 131.41, 130.71, 130.33, 127.36, 126.92, 125.91, 124.99, 123.09, 119.13, 118.91, 118.84, 118.73, 112.04, 71.80, 71.70, 39.08, 30.32, 28.97, 28.94, 23.66, 22.99, 22.97, 20.65, 14.01, 13.97, 10.94, 10.91 ppm.

IR (KBr, transmittance): ν = 3429, 3285, 3175, 2959, 2926, 2872, 2858, 1628, 1603, 1576, 1551, 1462, 1447, 1409, 1308, 1269, 1238, 1219, 1206, 1107, 1072, 1055, 1022, 972, 856, 820, 812, 785, 743, 700, 671, 662, 640, 621, 526 cm^{-1}.

HRMS (ESI): m/z calcd. for $C_{51}H_{49}N_2O_6S_2$: 849.3038, found: 849.3037 ($[M-H)^-$).

Results and Discussion

Synthesis

Attempts to couple a simple a simple anchoring unit furnished with a carboxylic acid to the BAI core in Figure 2 led to insoluble products. To reduce π-π stacking, the planar core was functionalised with sterically demanding 2-ethylhexyloxy groups prior to bay-annulation, following the procedure outlined in Figure 3.[27]

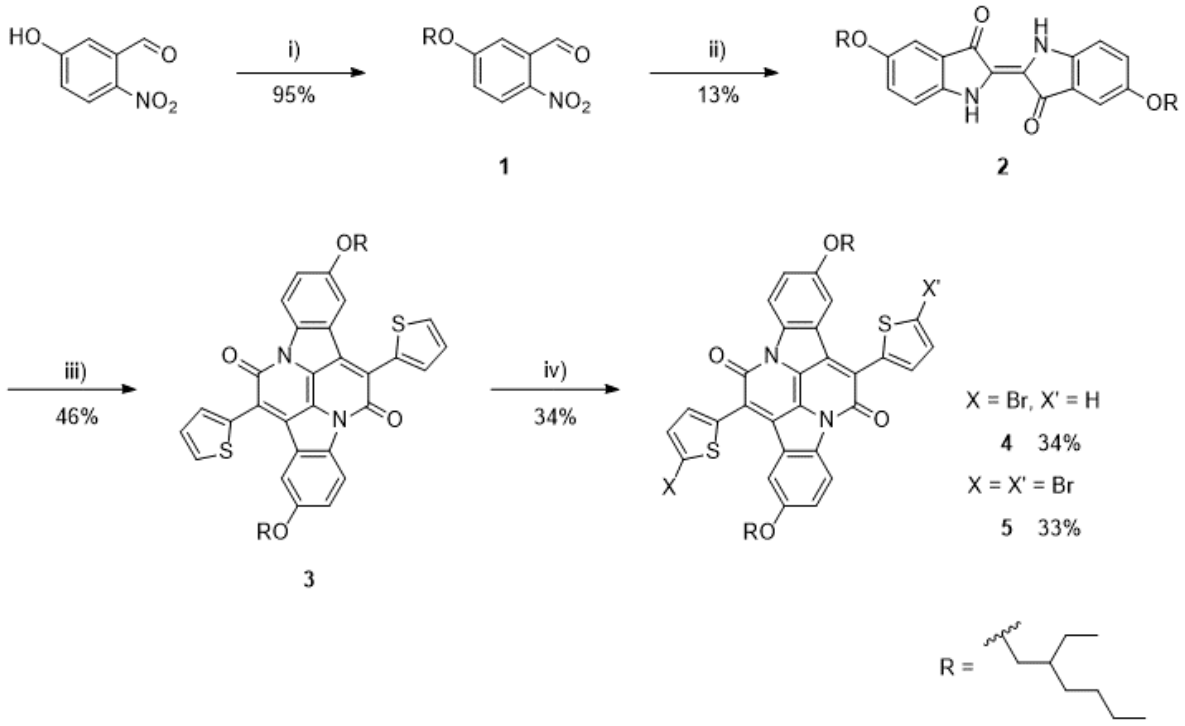

Figure 3. Synthesis and asymmetric halogenation of **3** i) 2-ethylhexyl bromide, K_2CO_3, 18-crown-6, DMF, 95%; ii) NaOH, acetone/water, 13%; iii) 2-thienylacetyl chloride, xylene, 46%; iv) NBS, $CHCl_3$, 34%.

The first step was the alkylation of 5-hydroxy-2-nitrobenzaldehyde using 2-ethylhexyl bromide, which produced **1** in 95% yield. **2** was produced by the Baeyer–Drewson reaction of **1** and acetone in 13% yield after recrystallisation. This was reacted with 2-thienylacetyl chloride in refluxing xylene to give the bay annulated product (**3**) in 46% yield after purification by recrystallisation. To avoid an asymmetric Suzuki coupling, **3** was brominated on one thiophene by reacting with a slight excess (1.1

eqv.) of NBS. While the reaction was not selective, the desired product (**4**) could be separated from the bis-brominated product (**5**) using column chromatography and was isolated in a yield of 34% (with **5** obtained in 33% yield as a by-product). Isolation of the mono-brominated molecule enables the introduction of the anchoring group via Suzuki coupling. For this initial study, to test the suitability of BAI-based dyes for pDSCs, a simple dye (**BAI-COOH**) was prepared from **4** and 4-carboxyphenylboronic acid (Figure 4). In the future, a second round of halogenation and coupling reactions could be used to introduce an acceptor group, based on the results obtained from this prototype dye.

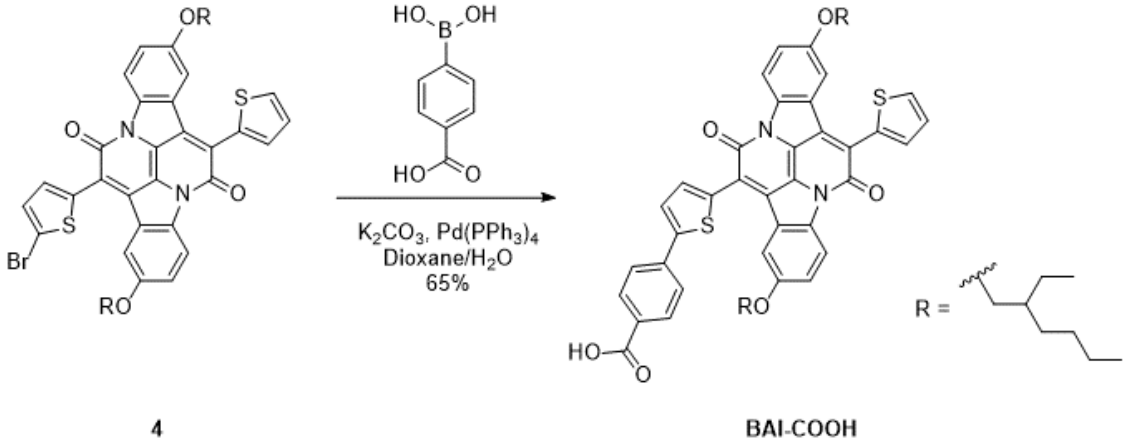

Figure 4. Synthesis of **BAI-COOH**.

When the starting material had been fully consumed, the solvent was evaporated and the crude residue was purified by column chromatography using a 95:5:1 toluene/methanol/acetic acid mixture, giving **BAI-COOH** in 65% yield. The product was confirmed using ^{1}H NMR spectroscopy, by the formation of two new 2H doublet peaks corresponding to benzoic acid at 8.18 and 7.84 ppm (Figure S2). While the solubility of the product from the Suzuki reaction between **4** and 4-carboxyphenylboronic acid was greatly decreased after the reaction, it was possible to achieve limited solubility for **BAI-COOH** in mixed solvent systems (such as $CHCl_3$/BuOH). The solubility could be further improved by adding acids or bases to the suspension of **BAI-COOH** in $CHCl_3$. Trifluoroacetic acid (TFA) and pyridine were chosen because of their solubility in organic solvents, e.g. $CHCl_3$. This suggests that the insolubility is primarily due to aggregation arising from hydrogen bonding interactions between the carboxylic acid and carbonyl groups (on both the acid group and the core).

Optical and Electrochemical Characterisation

As the dye was poorly soluble in pure solvents, the UV-visible absorption and emission spectra of **BAI-COOH** were measured in $CHCl_3$/TFA (99:1 v/v) and the results are shown in Figure 5, Figure S9 and

in Table 1. A linear relationship between concentration and absorption was observed over a concentration range of $1.16 \times 10^{-6} – 2.16 \times 10^{-5}$ M (Figure S10 and 11). The absorption and emission peak maxima are separated by a Stokes shift of 2323 cm^{-1}. The UV-visible absorption spectra of **BAI-COOH** compared to the symmetric core (**3**) is given in Figure S9 in the ESI. For **3**, the absorption maximum (584 nm) has been previously attributed to a π-π* transition and the shoulder (547 nm) to an intramolecular charge transfer transition. However, as the shoulder is also present in the emission spectra, we attribute it to vibrational fine structure. In comparison, the absorption spectrum of **BAI-COOH** is less well-defined and broader than **3**. This broad absorption band at longer wavelengths is particularly advantageous for tandem devices. When adsorbed onto NiO (Figure S20), there is a 22 nm hypsochromic shift of the absorption maxima (to 545 nm), which is possibly caused by deprotonation or interactions with the semiconductor upon binding.

Figure 6 shows the change in UV-visible absorption spectra of **BAI-COOH** recorded in $CHCl_3$/pyridine (10:1, v/v) across the same concentration range as Figure S10 and Figure S11. In contrast to the spectra in acidic solution, in the presence of pyridine, there is a non-linear relationship between concentration and absorption. As the concentration of **BAI-COOH** increases, an absorption band at 570 nm appears and becomes more intense. This is clearly seen in the normalised spectra (Figure S12 in the ESI), in which at higher concentrations this band becomes more intense than the π-π* transition at 610 nm.

The emission spectra in both acidic and basic conditions are roughly a mirror image of the absorption profile, but a shoulder is more prominent in the emission spectra. The emission spectra obtained from multiple excitation wavelengths were compared (Figure S13 in the ESI) and the shape of the emission band remained unchanged. A comparison of the normalised absorption and excitation spectra recorded for various emission wavelengths (Figure S14 in the ESI) show a reasonable agreement, indicating that the emissive species in each case originates from the same species. However, the excitation spectrum are slightly red-shifted and sharper than the absorption spectra, indicating that more than one species, one emissive and (at least) one non-emissive, are present.

In non-protic solvents, benzoic acid derivatives typically exist as hydrogen-bonded cyclic or acyclic dimers. Addition of TFA or pyridine is anticipated to disrupt dimer formation by forming adducts, improving the solubility. The hypsochromic shift observed in the presence of pyridine could be attributed to H-aggregation, which occurs when chromophores stack. H-aggregation, driven by π-interactions between molecules, has often been observed in perylenes which have a similar planar, conjugated aromatic core.[28,29] When increasing the concentration of rigid organic dyes, it is common for certain vibrational transitions to start to prevail over others as the dyes start to weakly interact with each other until an inversion of their relative intensities, as observed here.[30] H-aggregates are typically non-emissive, which is consistent with the comparison of the absorption and excitation spectra. It is not obvious why H-aggregation is pronounced in the presence of pyridine compared to TFA (possibly,

pyridine promotes π-stacking and defines the geometry of the aggregate conformation, or hydrogen bonding may increase the rigidity of the system and sharpen the bands). Más-Montoya and Jansen have described a similar hypsochromic shift, or change in the relative intensities of the first and second vibronic bands in thin films of structurally related thiophene–pyridine–diketopyrrolopyrrole molecules.[31] The authors found that small changes in the chemical structure and deposition conditions could be used to tune the aggregation phenomena and, hence, the photophysical properties. The low solubility of the dye prevented a more detailed investigation of aggregation for **BAI-COOH**. Nonetheless, these molecular interactions could, if controlled, be exploited in organic electronic devices by increasing the bandwidth and/or charge-transport properties.

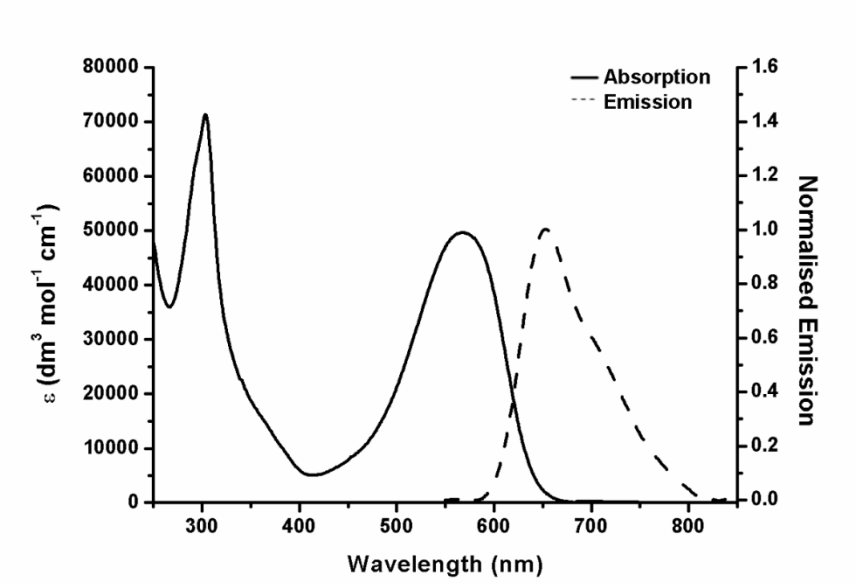

Figure 5. Normalised UV-visible absorption and emission spectra for **BAI-COOH** recorded in $CHCl_3$/TFA (99:1 v/v).

Table 1. UV-visible absorption and emission data for **BAI-COOH** in $CHCl_3$/TFA (99:1, v/v). Electrochemical data recorded using a glassy carbon electrode modified with **BAI-COOH** (deposited from a 2.16 x 10^{-5} M solution in $CHCl_3$/TFA (99:1 v/v)), a platinum counter electrode and a SCE reference electrode. The supporting electrolyte was 0.5 M TBA PF_6 in $CHCl_3$ and all potentials were calibrated and referenced vs. Fc/Fc^+.

λ_{abs} / nm (ε / M^{-1} cm^{-1})	λ_{em} (nm)	$E_{0\text{-}0}$[a] (eV)	$E_{1/2}$Ox (V)	$E_{1/2}$Red (V)	$E_{1/2}(S^*/S^-)$[b] (V)	ΔG_{inj}[c] (eV)	$\Delta G_{reg}(I^-/I_3^-)$[d] (eV)
567 (49650), 303 (71375)	653	2.00	0.93	-1.25	0.75	-0.87	-0.43

λ_{abs} is the wavelength of maximum absorption, λ_{em} is the wavelength of maximum emission, $E_{0\text{-}0}$ is the zero-zero energy, $E_{1/2}$Ox and $E_{1/2}$Red are the ground state oxidation and reduction potentials (as determined using DPV), $E_{1/2}(S^*/S^-)$ is the excited state reduction potential, ΔG_{inj} is the driving force for charge transfer from NiO to the excited dye and $\Delta G_{reg}(I^-/I_3^-)$ is the driving force for regeneration of the reduced dye. [a] Determined from the intersection of the normalised absorption and emission spectra. [b] Determined according to the equation: $E_{1/2}(S^*/S^-) = E_{1/2}\text{Red} + E_{0\text{-}0}$. [c] Determined according to the

equation: $\Delta G_{inj} = E_{VB}(NiO) - E_{1/2}(S^*/S^-)$, where $E_{VB}(NiO) \approx -0.12$ V vs. Fc.[23] [d] Determined according to the equation: $\Delta G_{reg}(I^-/I_3^-) = E(I_3^-/I_2^{\cdot-}) - E_{1/2}Red$, where $E(I_3^-/I_2^{\cdot-}) = -0.82$ V vs. Fc.[32]

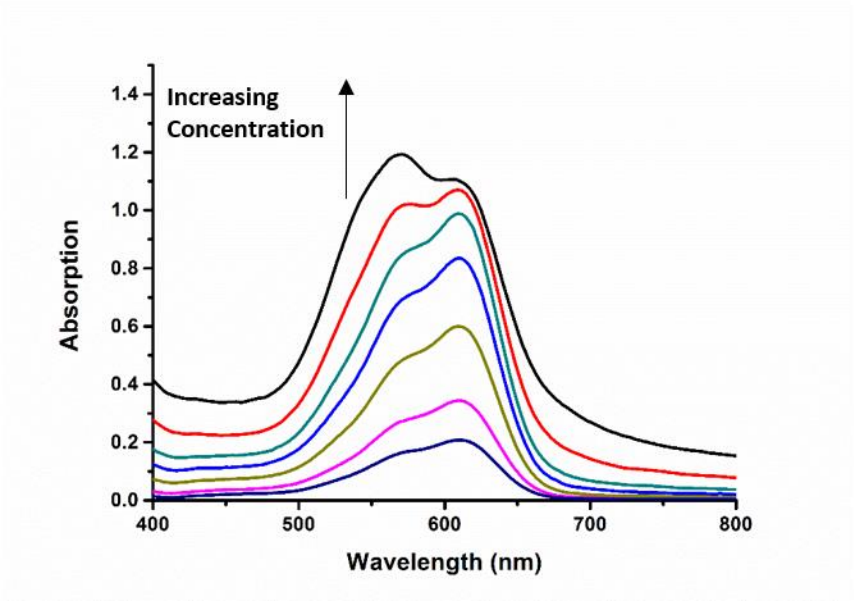

Figure 6. Overlaid UV-visible absorption spectra of **BAI-COOH** in $CHCl_3$/pyridine (10:1 v/v) with a concentration range of $1.16 \times 10^{-6} – 2.16 \times 10^{-5}$ M .

The ground state oxidation and reduction potentials of **BAI-COOH** were determined using DPV (Figure S17 and S18). As the dye was insoluble in single-solvent systems and a sufficiently high concentration could only be achieved through the addition of acids/bases, the electrochemistry was performed with **BAI-COOH** immobilised on a glassy carbon electrode (deposited from a 2.16×10^{-5} M solution in $CHCl_3$/TFA (99:1 v/v). From this study, the driving force for charge transfer from NiO to the excited dye (ΔG_{inj}) and dye regeneration (ΔG_{reg}) have been determined (Table 1). An estimated $\Delta G_{inj} = –0.87$ eV should be sufficient for photoinduced charge transfer from NiO to **BAI-COOH** to be efficient, based on the threshold of $\Delta G_{inj} > -0.8$ eV proposed by Liu *et al.*.[23] There must be a sufficient driving force for dye regeneration to compete with charge recombination between the reduced dye and NiO. The estimated ΔG_{reg} (**BAI-COOH**) = –0.43 eV is larger than for our champion dye **CAD3** (ΔG_{reg} = -0.17 eV) and thus should be sufficient to promote dye regeneration.[21]

Computational Studies

Density Functional Theory (DFT) calculations were used to determine the molecular orbital distributions within **BAI-COOH**, to visualise the electronic transitions that occur when the dye is excited. Theoretical energy levels and the corresponding molecular orbital distributions were calculated

using the hybrid B3LYP[33] exchange functional and a 6-31G(d,p) basis set. Solvation was treated using the polarisable continuum model (PCM). Initially, the ground state geometries were optimised (in $CHCl_3$) then frequency calculations were performed to check this was a true energy minimum. TDDFT calculations were then used to determine the vertical excitation energies.

The HOMO-LUMO orbital distributions alongside the calculated energy levels are given in Figure 7. Both the HOMO and LUMO are delocalised across the entire conjugated system and there is no 'push-pull' character within the molecule. This lack of a charge transfer to the periphery of the dye could be detrimental to pDSC performance, as there is little spatial separation to hinder charge recombination.

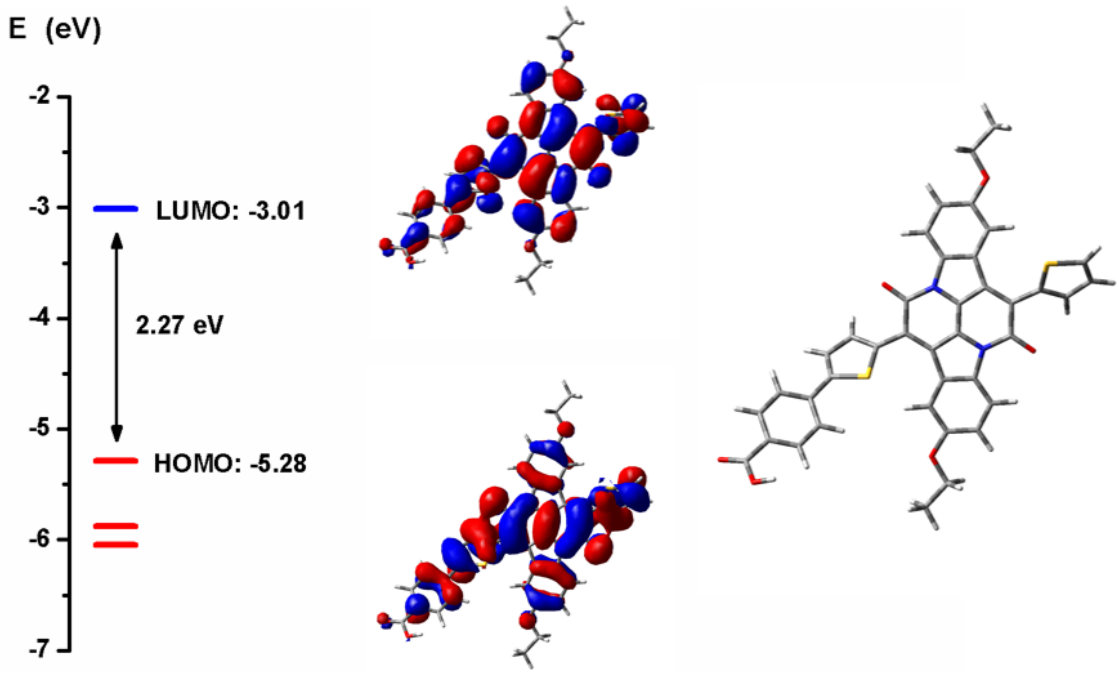

Figure 7. Optimised geometry, calculated energy level diagram and orbital distribution (top = LUMO, bottom = HOMO) for **BAI-COOH** in $CHCl_3$ using B3LYP/6-31G(d,p).

Table 2. Calculated singlet energy transitions for **BAI-COOH** determined by TDDFT (calculated using B3LYP/6-31G(d,p) in $CHCl_3$ using the PCM), their oscillator strengths (*f*) and the contributions from specific orbitals.

Energy / eV (λ / nm)	*f*	Composition (contribution / %)
2.0306 (611)	0.9914	H → L (99)
2.5441 (487)	0.0103	H - 2 → L (97)

TTDFT was used to calculate the electronic transitions which were compared to the experimental data. The calculated transitions are summarised in Table 2 and a comparison of the calculated and

experimental transitions is given in Figure S19 in the ESI. There is a good agreement between the calculated lowest energy excitation and the experimentally obtained absorption maxima for **BAI-COOH**. This transition corresponds with a HOMO to LUMO π-π* transition, which has very little charge transfer character. A weaker transition at higher energy is attributed to a HOMO-2 to LUMO transition, which has more charge transfer character as the HOMO-2 orbital is predominantly located on the benzoic acid anchor and nearest thiophene. Here there is more of a shift in electron density onto the conjugated core. However, the calculated intensity is ten times lower than for the major transition.

Device Performance

The performance of **BAI-COOH** assembled in a pDSC was tested and compared to similar structures in the literature, alongside **P1** as a benchmark. Devices were constructed from **BAI-COOH** and **P1** by immersing 1.5 µm thick NiO films in a solution of the dye for 16 hours (0.3 mM in MeCN for **P1** and a saturated solution in 1:1 v/v $CHCl_3$/BuOH containing 1 mM chenodeoxycholic acid for **BAI-COOH**). This dye bath was chosen to optimise dye loading on the NiO surface. The electrolyte used was 1.0 M LiI and 0.1 M I_2 in MeCN. The performances are summarised in Table 3.

Table 3. Photovoltaic performance of p-DSCs constructed using **BAI-COOH** and **P1** using NiO films from the same batch. Standard deviations for J_{sc}, V_{oc}, FF and η, as determined for four devices, are given in parenthesis.

	J_{SC} / mA cm^{-2}	V_{OC} / mV	FF	η / %	IPCE / %	APCE / %
BAI-COOH	1.13 (0.22)	79 (2.4)	0.33 (0.003)	0.029 (5.9×10^{-4})	7.8	10.4
P1	1.93 (0.28)	99 (7.5)	0.33 (0.02)	0.063 (9.9×10^{-3})	31.0	32.6

J_{sc} is the short-circuit current density at the $V = 0$ intercept, V_{oc} is the open-circuit voltage at the $J = 0$ intercept, *FF* is the device fill factor, η is the power conversion efficiency, IPCE is the monochromatic incident photon-to-current conversion efficiency and APCE is the monochromatic absorbed photon-to-current conversion efficiency.

The J-V curves of the highest performing devices are given measured under illumination (Figure 8 (a)) and in the dark (Figure 8 (b)). From the J-V curves measured under illumination it is apparent that **BAI-COOH** performs modestly, but worse than **P1**. However, there is room for optimisation here, as the results for **P1** are lower than the reported record.[34] This could be done by optimising the film preparation or electrolyte composition. The V_{OC} obtained for **BAI-COOH** is lower than for **P1**, which

could partly be due to increased recombination between the electrolyte and NiO. This is supported by the higher dark currents for **BAI-COOH** than **P1** (Figure 8 (b)). While the aliphatic chains present on **BAI-COOH** should inhibit electrolyte/NiO recombination,[35,36] lower dye loading (see below) could counter this effect. Despite performing worse than **P1**, the cell results for **BAI-COOH** are higher than the structurally related 'first-generation' DPP dyes (**DPP-Br/Th-DPP**),[5,37] which shows that BAI is a promising chromophore on which to base a more structurally complex dye.

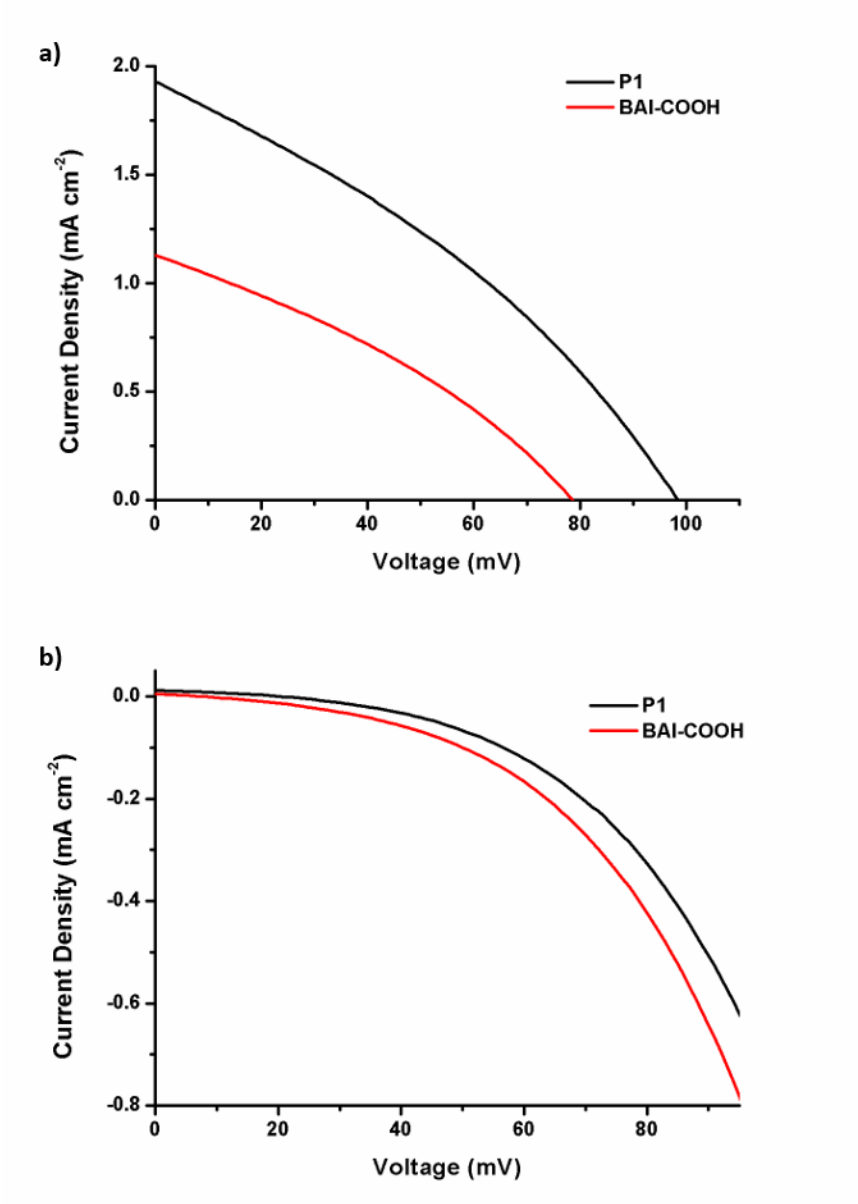

Figure 8. J-V curves of pDSCs constructed using **BAI-COOH** (red) and **P1** (black), (a) measured under illumination (AM1.5, 100 mW cm^{-2}), (b) measured in the dark.

The IPCE spectra for **BAI-COOH** and **P1** are given in Figure 9. The spectral shape (maxima at 550 nm) is consistent with excitation of the dye contributing to the photocurrent and the lower magnitude for **BAI-COOH** compared to **P1** (ca. 8% vs 31%) agrees with the lower J_{SC}. Most of the photocurrent

produced from cells made using **BAI-COOH** comes from the photodissociation of triiodide (the band < 450 nm),[32] whereas for **P1** the shape of the spectral response matched the absorption spectrum of the dye. One reason for the lower IPCE is a lower LHE, as the NiO film sensitised with **BAI-COOH** has a lower optical density than for **P1** (*A* = 1.2 for **BAI-COOH** vs. *A* = 1.6 for **P1**, Figure S23). This is reflected in the higher APCE/IPCE ratio for **BAI-COOH** than **P1.**

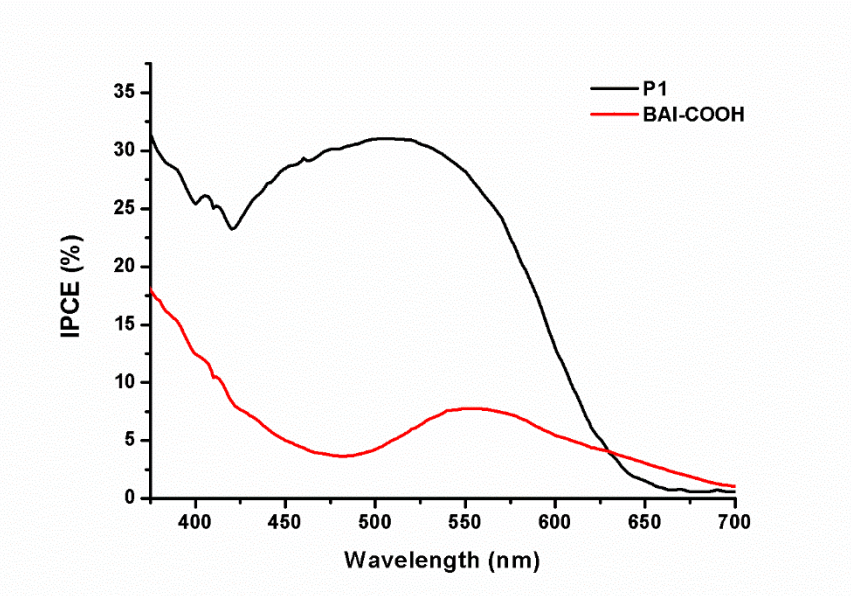

Figure 9. IPCE spectra of pDSCs constructed using **BAI-COOH** and **P1**.

The charge density and lifetime in the devices were analysed using charge extraction and small amplitude square wave modulated photovoltage experiments and are shown in Figure 10.[38] At the same charge-density, the V_{OC} is slightly higher for **BAI-COOH** than **P1**, which suggest that the Fermi level is slightly deeper. This is typically associated with a positive shift in the valence band edge. However, this is opposite to the trend that was anticipated from the dark current curves. Figure 10 (b) shows that, at the same charge density, the charge lifetime is longer for **BAI-COOH** than **P1**. This suggests that recombination between holes in the NiO with the reduced species in the electrolyte is slower for **BAI-COOH** than **P1**. Disappointingly, this does not increase the V_{OC} at 1 sun illumination. Reasons for this could be that fewer charges are injected into the NiO, or charge-recombination between the reduced dye with charges in the NiO could be faster for **BAI-COOH** compared to **P1.**

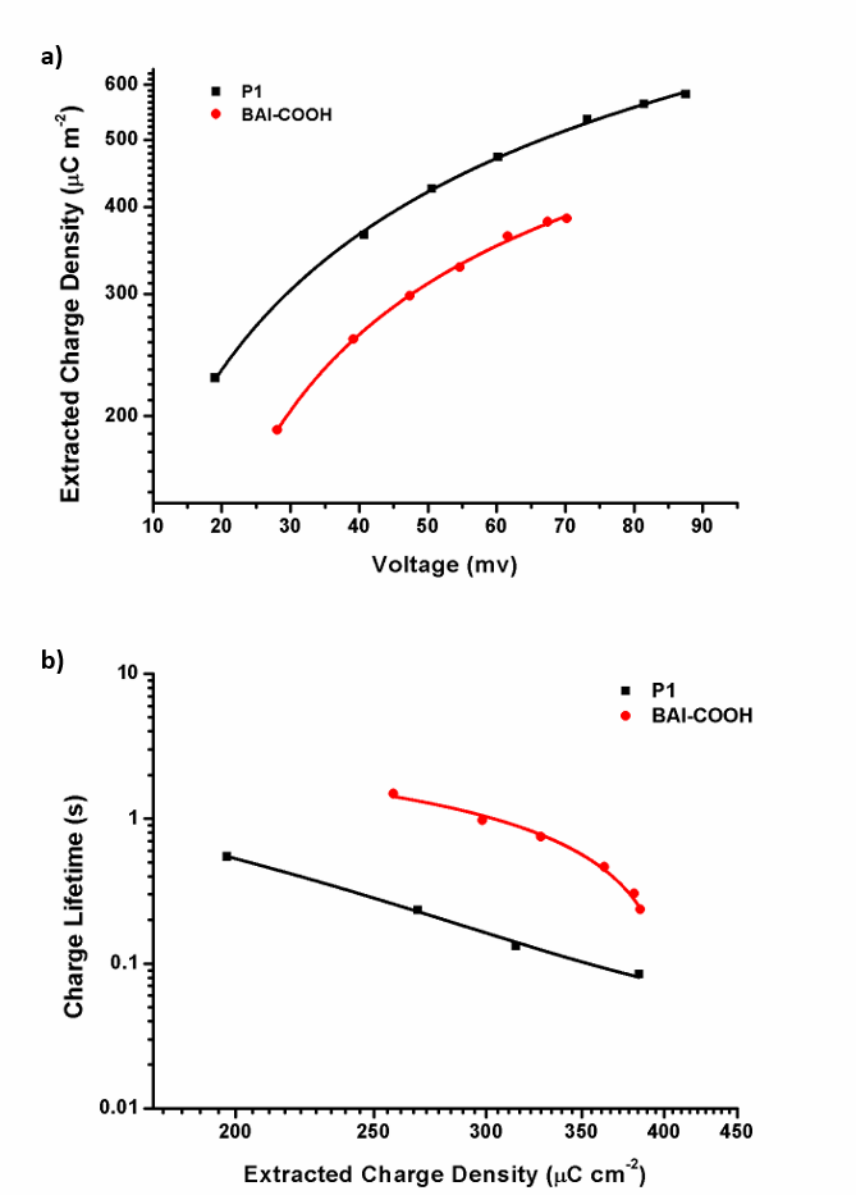

Figure 10 (a). Extracted charge density as a function of photovoltage and (b) charge lifetime as a function of extracted charge density for pDSCs constructed using **BAI-COOH** (red) and **P1** (black).

A possible limiting factor to the efficiency of pDSCs constructed using **BAI-COOH** is a low dye-loading compared to **P1**. Assuming that the extinction coefficient of the immobilised dye is not significantly changed from the values calculated from solution, dye loading can be calculated from the following equation:

$$\Gamma pro = A(\lambda)/1000 \times \varepsilon(\lambda).$$

Γpro is the number of moles of dye per square centimetre of projected surface area (mol cm^{-2}), A is the film absorbance and ε is the molar extinction coefficient for the dye in solution.[39]

Using 58000 M^{-1} cm^{-1} as the extinction coefficient for **P1**,[12] dye loading was estimated as 22.4 nmol cm^{-2}. In comparison, **BAI-COOH** had a lower dye loading of 12.1 nmol cm^{-2}. The branched ethylhexyl chains were necessary to improve the solubility of the BAI core, to allow functionalisation with an anchoring group. However, in addition to the limited solubility of **BAI-COOH** in the dye-bath solvent, the added steric bulk likely contributed to the low dye loading. This will reduce the LHE of the device, which will reduce the photocurrents produced.

While the pDSC performances of **BAI-COOH** were quite low compared to the champion dye **P1**, it outperforms the structurally similar DPP dyes developed by Odobel *et al*. (J_{sc} = 0.88 mA cm^{-2} and IPCE = 6% for **DPP-Br**; J_{sc} = 0.26 mA cm^{-2} and IPCE = < 5% for **Th-DPP**)[40,41] For these dyes, appending a napthalenediimide acceptor increases the current to J_{SC} = 7.38 mA cm^{-2}. It is anticipated that a similar strategy could be applied to **BAI** dyes to improve the performance.

Conclusions

The BAI chromophore has a number of advantageous properties, including large absorption coefficient, appropriate energy level alignment and absorption in the red region of the visible spectrum, which make it attractive for applications in tandem dye-sensitized solar cells. A prototype dye, **BAI-COOH**, based on a BAI core, containing solubilising branched alkyl chains, was successfully furnished with an anchoring group that allowed covalent bonding to NiO. The 2-ethylhexyl substituents improved the solubility compared to the unsubstituted dye, but were insufficient to prevent aggregation in solution. Addition of acid or base to the $CHCl_3$ solution improved the solubility, but above μM concentrations, H-aggregates were observed in the presence of pyridine. The dye was applied in p-type dye-sensitized solar cells and the promising photocurrent density (Jsc = 1.13 mA cm^{-2}) generated was higher than the first-generations of structurally similar dyes reported elsewhere. The challenges to improving the performance include increasing the solubility and limiting the aggregation of the dye, in addition to improving the charge-transfer character. Further work to append an electron acceptor, such as napthalenediimide, to slow down back-electron transfer to the NiO and bulkier substituents on the π-linker is anticipated to improve the performance.

Acknowledgements

EAG gratefully acknowledges the Royal Society for funding a Dorothy Hodgkin Research Fellowship. GHS thanks Newcastle University for a PhD studentship. We thank the EPSRC UK National Mass Spectrometry Facility at Swansea University. Thanks to Fabio Cucinotta for insightful discussions.

References

[1] B. O'Regan, M. Grätzel, *Nature* **1991**, *353*, 737–740.

[2] A. Yella, H.-W Lee, H. N. Tsao, C. Yi, A. K. Chandiran, M. K. Nazeeruddin, E. W.-G. Diau, C.-Y. Yeh, S. M. Zakeeruddin, M. Gratzel, *Science.* **2011**, *334*, 629–634.

[3] S. Mathew, A. Yella, P. Gao, R. Humphry-Baker, B. F. E. Curchod, N. Ashari-Astani, I. Tavernelli, U. Rothlisberger, M. K. Nazeeruddin, M. Grätzel, *Nat. Chem.* **2014**, *6*, 242–247.

[4] K. Kakiage, Y. Aoyama, T. Yano, K. Oya, J. Fujisawa, M. Hanaya, *Chem. Commun.* **2015**, *51*, 15894–15897.

[5] Y. Farré, M. Raissi, A. Fihey, Y. Pellegrin, E. Blart, D. Jacquemin, F. Odobel, *ChemSusChem* **2017**, 10, 2618-2625.

[6] J. He, H. Lindström, A. Hagfeldt, S. Lindquist, *J. Phys. Chem. B* **1999**, *103*, 8940–8943.

[7] I. R. Perera, T. Daeneke, S. Makuta, Z. Yu, Y. Tachibana, A. Mishra, P. Bäuerle, C. A. Ohlin, U. Bach, L. Spiccia, L. *Angew. Chemie* **2015**, *127*, 3829–3833.

[8] F. Odobel, Y. Pellegrin, E. A. Gibson, A. Hagfeldt, A. L. Smeigh, L. Hammarström, *Coord. Chem. Rev.* **2012**, *4*, 2551–2564.

[9] D. Dini, Y. Halpin, J. G. Vos, E. A. Gibson, *Coord. Chem. Rev.* **2015**, *304–305*, 179–201.

[10] T. Daeneke, Z. Yu, G. P. Lee, D. Fu, N. W. Duffy, S. Makuta, Y. Tachibana, L. Spiccia, A. Mishra, P. Bäuerle, U. Bach, *Adv. Energy Mater.* **2015**, *5*, 1401387.

[11] Z. Huang, G. Natu, Z. Ji, M. He, M. Yu, Y. Wu, *J. Phys. Chem. C* **2012**, *116*, 26239–26246.

[12] P. Qin, J. Wiberg, E. A. Gibson, M. Linder, L. Li, T. Brinck, A. Hagfeldt, B. Albinsson, L. Sun, *J. Phys. Chem. C* **2010**, *114*, 4738–4748.

[13] A. Nattestad, A. J. Mozer, M. K. R. Fischer, Y.-B. Cheng, A. Mishra, P. Bäuerle, U. Bach, *Nat. Mater.* **2010**, *9*, 31–35.

[14] Y. Pellegrin, L. Le Pleux, E. Blart, A. Renaud, B. Chavillon, N. Szuwarski, M. Boujtita, L. Cario, S. Jobic, D. Jacquemin, F. Odobel, *J. Photochem. Photobiol. A Chem.* **2011**, *219*, 235–242.

[15] F. Brunner, N. Marinakis, C. Wobill, M. Willgert, C. D. Ertl, T. Kosmalski, M. Neuburger, B.

Bozic-Weber, T. Glatzel, E. C. Constable, C. E. Housecroft, *J. Mater. Chem. C* **2016**, *4*, 9823–9833.

[16] J. Cui, J. Lu, X. Xu, K. Cao, Z. Wang, G. Alemu, H. Yuang, Y. Shen, J. Xu, Y.-B. Cheng, M. Wang, *J. Phys. Chem. C* **2014**, *118*, 16433–16440.

[17] Y. Dong, L. Wei, R. Fan, Y. Yang, P. Wang, *RSC Adv.* **2016**, *6*, 39972–39981.

[18] G. Alemu, J. Cui, K. Cao, J. Li, Y. Shen, M. Wang, *RSC Adv.* **2014**, *4*, 51374–51380.

[19] D'Amario, L.; Antila, L. J.; Pettersson Rimgard, B.; Boschloo, G.; Hammarström, L. *J. Phys. Chem. Lett.* **2015**, *6* (5), 779–783.

[20] R. J. Dillon, L. Alibabaei, T. J. Meyer, J. M. Papanikolas, *ACS Appl. Mater. Interfaces* **2017**, *9*, 26786–26796.

[21] C. J. Wood, G. H. Summers, E. A. Gibson, *Chem. Commun.* **2015**, *51*, 3915–3918.

[22] P. Qin, PhD Thesis, The Study of Organic Dyes for p-Type Dye- Sensitized Solar Cells, KTH: Stockholm, 2010.

[23] Z. Liu, W. Li, S. Topa, X. Xu, X. Zeng, Z. Zhao, M. Wang, W. Chen, F. Wang, Y.-B. Cheng, H. He, *ACS Appl. Mater. Interfaces* **2014**, *6*, 10614–10622.

[24] D. Ameline, S. Diring, Y. Farre, Y. Pellegrin, G. Naponiello, E. Blart, B. Charrier, D. Dini, D. Jacquemin, F. Odobel, *RSC Adv.* **2015**, *5*, 85530–85539.

[25] B. He, A. B. Pun, D. Zherebetskyy, Y. Liu, F. Liu, L. M. Klivansky, A. M. McGough, B. A. Zhang, K. Lo, T. P. Russell, L. Wang, Y. Liu, *J. Am. Chem. Soc.* **2014**, *136*, 15093–15101.

[26] J. Seixas de Melo, A. P. Moura, M. J. Melo, *J. Phys. Chem. A* **2004**, *108*, 6975–6981.

[27] B. He, W. T. Neo, T. L. Chen, L. M. Klivansky, H. Wang, T. Tan, S. J. Teat, J. Xu, Y. Liu, *ACS Sustain. Chem. Eng.* **2016**, *4*, 2797–2805.

[28] S. Yagai, T. Seki, T. Karatsu, A. Kitamura, F. Würthner, *Angew. Chemie - Int. Ed.* **2008**, *47*, 3367–3371.

[29] H. Langhals, *Helv. Chim. Acta* **2005**, *88*, 1309–1343.

[30] F. C. Spano, *Acc. Chem. Res.* **2010**, *43*, 429–439.

[31] M. Más-Montoya, R. A. J. Janssen, *Adv. Funct. Mater.* **2017**, *27*, 1605779.

[32] E. A. Gibson, L. Le Pleux, J. Fortage, Y. Pellegrin, E. Blart, F. Odobel, A. Hagfeldt, G. Boschloo, *Langmuir* **2012**, *28*, 6485–6493.

[33] A. D. Becke, *J. Chem. Phys.* **1993**, *98*, 1372.

[34] L. Li, E. A. Gibson, P. Qin, G. Boschloo, M. Gorlov, A. Hagfeldt, L. Sun, *Adv. Mater.* **2010**, *22*, 1759–1762.

[35] C. J. Wood, M. Cheng, C. A. Clark, R. Horvath, I. P. Clark, M. L. Hamilton, M. Towrie, M. W. George, L. Sun, X. Yang, E. A. Gibson, *J. Phys. Chem. C* **2014**, *118*, 16536–16546.

[36] K. A. Click, D. R. Beauchamp, B. R. Garrett, Z. Huang, C. M. Hadad, Y. Wu, *Phys. Chem. Chem. Phys.* **2014**, *16*, 26103–26111.

[37] L. Favereau, J. Warnan, Y. Pellegrin, E. Blart, M. Boujtita, D. Jacquemin, F. Odobel, *Chem. Commun.* **2013**, *49*, 8018.

[38] N. Duffy, L. Peter, R. M. Rajapakse, U. K. G. Wijayantha, *Electrochem. Commun.* **2000**, *2*, 658–662.

[40] S. A. Trammell, T. J. Meyer, *J. Phys. Chem. B* **1999**, *103*, 104–107.

[41] Y. Farré, L. Zhang, Y. Pellegrin, A. Planchat, E. Blart, M. Boujtita, L. Hammarström, D. Jacquemin, F. Odobel, *J. Phys. Chem. C* **2016**, *120*, 7923–7940.

Keywords

Dye-sensitized solar cell, p-type, tandem, artificial photosynthesis, indigo, nickel oxide.

Table of Contents text

We present a new bay-annulated indigo dye applied in p-type dye-sensitized solar cells. The dye is furnished with a carboxylic acid anchoring group and branched aliphatic substituents to reduce stacking at the NiO surface. The promising spectral response in the red region is encouraging for applications in tandem cells.


OR
O
N
S
O
N
S
RO
R =
HO
O
BAI-COOH